SCIENTIFIC REPORTS
nature research

OPEN

Sorting Fermionization from Crystallization in Many-Boson Wavefunctions

S. Bera[1], B. Chakrabarti[1,2], A. Gammal[2], M. C. Tsatsos[3], M. L. Lekala[4], B. Chatterjee[5], C. Lévêque[6,7] & A. U. J. Lode[6,7,8*]

Fermionization is what happens to the state of strongly interacting repulsive bosons interacting with contact interactions in one spatial dimension. Crystallization is what happens for sufficiently strongly interacting repulsive bosons with dipolar interactions in one spatial dimension. Crystallization and fermionization resemble each other: in both cases – due to their repulsion – the bosons try to minimize their spatial overlap. We trace these two hallmark phases of strongly correlated one-dimensional bosonic systems by exploring their ground state properties using the one- and two-body density matrix. We solve the *N*-body Schrödinger equation accurately and from first principles using the multiconfigurational time-dependent Hartree for bosons (MCTDHB) and for fermions (MCTDHF) methods. Using the one- and two-body density, fermionization can be distinguished from crystallization in position space. For *N* interacting bosons, a splitting into an *N*-fold pattern in the one-body and two-body density is a unique feature of both, fermionization and crystallization. We demonstrate that this splitting is incomplete for fermionized bosons and restricted by the confinement potential. This incomplete splitting is a consequence of the convergence of the energy in the limit of infinite repulsion and is in agreement with complementary results that we obtain for fermions using MCTDHF. For crystalline bosons, in contrast, the splitting is complete: the interaction energy is capable of overcoming the confinement potential. Our results suggest that the spreading of the density as a function of the dipolar interaction strength diverges as a power law. We describe how to distinguish fermionization from crystallization experimentally from measurements of the one- and two-body density.

The physics of the ultracold Bose gas in one spatial dimension is strongly different from that of its three-dimensional counterpart[1,2]. In one spatial dimension, quantum effects are much more prominent. When the interactions are strong, quantum fluctuations are enhanced. Experimentally, in cold atom systems, the dimensionality can be manipulated using a tight transversal confinement that essentially freezes the radial degrees of freedom[3,4]. Such quasi-one dimensional systems display intriguing physics that cannot be realized for three-dimensional systems: *Fermionization*, occurs for strongly interacting bosons with contact interactions[5–12] and *crystallization* emerges for sufficiently strongly interacting bosons with dipole-dipole interactions[13–19]. For bosons with contact interactions, fermionization leads to the formation of the Tonks-Girardeau (TG) gas when the interaction strength tends to infinity. This is a consequence of the Bose-Fermi mapping[7,20–22] which implies that strongly interacting bosons and non-interacting spinless fermions have the same (one-body) density in position space. With increasing interaction strength, not only the density, but also the energy of fermionized bosons saturates to the energy of non-interacting fermions.

[1]Department of Physics, Presidency University, 86/1 College Street, Kolkata, 700 073, India. [2]Instituto de Física, Universidade de São Paulo, CEP 05508-090, São Paulo, Brazil. [3]Instituto de Física de São Carlos, Universidade de São Paulo, CP 369, 13560-970, São Carlos, SP, Brazil. [4]Department of Physics, University of South Africa P.O. Box-392, Pretoria, 0003, South Africa. [5]Department of Physics, Indian Institute of Technology-Kanpur, Kanpur, 208016, India. [6]Wolfgang Pauli Institute c/o Faculty of Mathematics, University of Vienna, Oskar-Morgenstern Platz 1, 1090, Vienna, Austria. [7]Vienna Center for Quantum Science and Technology, Atominstitut, TU Wien, Stadionallee 2, 1020, Vienna, Austria. [8]Institute of Physics, Albert-Ludwig University of Freiburg, Hermann-Herder-Strasse 3, 79104, Freiburg, Germany. *email: auj.lode@gmail.com

In the case of dipolar interactions, the remarkable phenomenon of crystallization occurs when the interaction strength is sufficiently large. Bosons interacting via a dipole-dipole interaction potential have become the primary cold atom system to investigate the many-body physics triggered as consequence of long-range interactions[23–28]. The long-ranged and anisotropic nature of the dipolar interaction potential results in a variety of interesting effects and phenomena[29], like crystallization in one- and two-dimensional systems[13–18,30–32], that are completely different from the emergent phenomena in the case of strong contact interactions. Crystallization is a consequence of the repulsive and long-ranged tail of the dipolar interactions dominating the physics[33,34]: the bosons maximally separate and minimize their spatial overlap. Unlike in the fermionization of bosons with strong contact interactions, the energy of crystallized bosons does not saturate. We note here that it is formally possible to define and measure an order parameter which is a function of the eigenvalues of the reduced one-body density matrix that allows to unequivocally identify the crystal phase of one-dimensional dipolar bosons[34]. Furthermore, we note that the formation of a crystal state is a generic feature of many-body systems of particles with long-ranged interactions. Fermions with long-ranged interactions, for instance, form a so-called Wigner crystal[19,35].

In this work, we analyze the differences between fermionized and crystallized bosons' wavefunctions using the energy as well as the one-body and two-body reduced density matrix. We demonstrate how fermionization can be distinguished from crystallization by quantifying the (experimentally accessible) spread of the one-body and two-body densities. The different spreading characteristics of the one-body and two-body densities for fermionized as compared to crystallized bosons are a direct consequence of the different behavior of the energy as a function of interaction strengths. For dipolar interactions the energy as a function of interaction strength is unbounded; this is in stark contrast to the bounded energy as a function of interactions for contact interactions. Current experimental setups, for instance, for Erbium[36], Erbium-Erbium molecules[37], or Sodium-Potassium molecules[38], enable the experimental exploration of systems with dominant dipole-dipole interactions needed for probing the physics of crystallization.

The (momentum) densities of bosons with dipolar interactions have been compared to those of fermions with dipolar interactions in Ref.[18]. Going beyond Ref.[18], we compare and quantify the spreading of the full density matrices of bosons with dipolar interactions to the spreading of the density matrices of bosons with contact interactions. We note that Ref.[39] discusses and compares the physics of spin-1/2 fermions with contact and with long-ranged interactions in lattices using a Hubbard description. Our work complements the findings in Ref.[39] by providing a comparison of single-component ("spin-0") bosons with contact and long-ranged dipolar interactions in continuous space without a lattice and without resorting to a Hubbard-tight-binding-description.

Fermionization and crystallization entail the breakdown of mean-field approaches like the time-dependent Gross-Pitaevskii (GP) equation[40–42]. To go beyond the GP approximation, multiconfigurational methods are employed[43–49]. Variational calculations using parametrized Gaussian functions as single-particle states have been successfully applied to investigate the crystallization of few particles in two dimensions[30,50,51]. Here, we use the multiconfigurational time-dependent Hartree for bosons (MCTDHB)[43,44] and fermions (MCTDHF)[46] methods implemented in the MCTDH-X software package[46,52–54] to compute the ground state of the few-particle Schrödinger equation, see Ref.[49] for a Review. While the MCTDHB method aims at solving the time-dependent Schrödinger equation for a many-body system, using imaginary time-propagation provides the ground-state of the system variationally, equivalent to the work of Ref.[55].

We illustrate our findings with computations for $N=4$ bosons in a parabolic trapping potential and trace the complete range of dipolar and contact interaction strengths by obtaining highly accurate results with MCTDHB.

This paper is structured as follows: in Sec. 2, we discuss the Hamiltonian and quantities of interest, in Sec. 3, we introduce the numerical method, MCTDHB, that we use for obtaining solutions of the few-body Schrödinger equation, in Sec. 4 we analyze fermionized and crystallized bosonic few-body states and discuss how they can be sorted from each other and we conclude our paper in Sec. 5. Results for other observables and an assessment of the accuracy of our computations with the exact diagonalization and MCTDHF approaches are collected in the Appendices 6 and 7.

Hamiltonian, One- and Two-Body Density

In order to discuss the stationary properties of the ground state (GS) of crystalline and fermionized bosons, we consider the time-independent many-body Schrödinger equation,

$$\hat{H}|\Psi\rangle = E|\Psi\rangle. \tag{1}$$

Here, $|\Psi\rangle$ is the many-body ground state, E its energy, and $\hat{H}$ the N-particle Hamiltonian in dimensionless units[56],

$$H = \sum_{i=1}^{N}\left(-\frac{1}{2}\frac{\partial^2}{\partial x_i^2} + V(x_i)\right) + \sum_{i<j} W(x_i - x_j), \tag{2}$$

where we set $V(x_i) = \frac{1}{2}x_i^2$ to be the external harmonic trap. The term $W(x_i - x_j)$ is the interaction potential. All quantities are dimensionless and expressed in harmonic oscillator units. To ensure that the system is in the quasi-1D regime, we assume strong confinement in the transversal direction, providing a cigar-shaped atomic density. The contact interactions read,

$$W(x_i - x_j) = \lambda\delta(x_i - x_j), \tag{3}$$

where λ is the interaction strength determined by the scattering length a_s and the transverse confinement frequencies[57]. For long-ranged dipolar interactions, we have

$$W(x_i - x_j) = \frac{g_d}{|x_i - x_j|^3 + \alpha}, \tag{4}$$

where g_d is the dipolar interaction strength and α is a short-range cut-off to avoid the divergence at $x_i = x_j$. Repulsive interactions could be obtained in a quasi-1D BEC by imposing an external magnetic field to align all the dipole moments of the atoms[18]. This simple approximation to the one-dimensional dipole-dipole interaction potential in Eq. (4) is justified for the moderate to large interaction strengths and large inter-particle distance with respect to the harmonic-length of the transversal confinement[14,15,18,19,58], that we focus on in the present work. For such interaction strengths the dipole-dipole interaction potential is well-approximated by the $|x_i - x_j|^{-3}$ tail in Eq. (4), see[59]. Moreover, we have verified the consistency of the approximation in Eq. (4) for the same choice of cutoff parameter, $\alpha = 0.05$, by a direct comparison to a dipole-dipole interaction augmented with an additional contact interaction potential, see Ref.[34]. A rigorous discussion of the dipole-dipole interaction potential in one and two spatial dimensions can be found in Ref.[59]. Here, for the sake of simplicity, we will focus on quasi-one-dimensional systems, with $N = 4$ interacting bosons for all our calculations and consider repulsive interactions, i.e., $\lambda > 0$ and $g_d > 0$, exclusively.

In the following we discuss the reduced one-body density matrix, defined as

$$\rho^{(1)}(x, x') = \langle \Psi | \hat{\psi}^\dagger(x') \hat{\psi}(x) | \Psi \rangle. \tag{5}$$

Its diagonal,

$$\rho(x) \equiv \rho^{(1)}(x, x' = x) \tag{6}$$

is simply the one-body density. As a precursor of correlation effects that may be present in the state $|\Psi\rangle$ of the system, we use the eigenvalues $\rho_i^{(NO)}$ of the reduced one-body density matrix $\rho^{(1)}$ in Eq. (5). For this purpose, we write $\rho^{(1)}$ in its eigenbasis:

$$\rho^{(1)}(x, x') = \sum_i \rho_i^{(NO)} \Phi_i^*(x') \Phi_i(x). \tag{7}$$

The eigenvalues $\rho_i^{(NO)}$ and eigenfunctions $\Phi_i(x)$ are referred to as natural occupations and natural orbitals, respectively. If only a single eigenvalue $\rho_i^{(NO)}$ is macroscopic, then the state $|\Psi\rangle$ describes a Bose-Einstein condensate[60]. The case when multiple eigenvalues $\rho_i^{(NO)}$ are comparable to the number of particles N is referred to as fragmentation[43,44,53,54,61–63].

In the following, we will also use the two-body density $\rho^{(2)}$ to characterize crystallization and fermionization. It is defined as

$$\rho^{(2)}(x_1, x_2) = \langle \Psi | \hat{\psi}^\dagger(x_1) \hat{\psi}^\dagger(x_2) \hat{\psi}(x_1) \hat{\psi}(x_2) | \Psi \rangle. \tag{8}$$

The two-body density quantifies the probability to detect two particles at positions x_1 and x_2.

Numerical Method

The computation of the exact many-body wave function is a difficult problem. To attack the many-body Schrödinger equation, Eq. (1), we use the time-dependent Schrödinger equation,

$$i\partial_t |\Psi\rangle = \hat{H} |\Psi\rangle, \tag{9}$$

with a Wick's rotation $t \to -i\tau$, i.e., a propagation with imaginary time. We expand the many-body wavefunction $|\Psi\rangle$ of N interacting bosons in a complete set of time-dependent permanents $|\vec{n}; t\rangle = |n_1, \ldots, n_M; t\rangle$ with at most M single-particle states or orbitals. The MCTDHB ansatz for the many-body wave function is thus

$$|\Psi(t)\rangle = \sum_{\vec{n}} C_{\vec{n}}(t) |\vec{n}; t\rangle. \tag{10}$$

Here, the permanents $|\vec{n}; t\rangle$ are symmetrized bosonic many-body states that are also referred to as "configurations". The sum in Eq. (10) runs on all configurations $\vec{n}$ of N particles in M orbitals. The number of permanents and coefficients $C_{\vec{n}}(t)$ is $N_{conf} = \binom{N + M - 1}{N}$. In second quantized representation the permanents are given as

$$|\bar{n}; t\rangle = |n_1, \ldots n_M; t\rangle = \left(\prod_{i=1}^{M} \frac{(\hat{b}_i^\dagger(t))^{n_i}}{\sqrt{n_i!}} \right) |vac\rangle. \tag{11}$$

Here $\hat{b}_k^\dagger(t)$ is the bosonic creation operator which creates a boson in the time-dependent single particle state $\phi_k(x, t)$. Equation (10) spans the full N-body Hilbert space in the limit of $M \to \infty$. For practical computations, we restrict the number of orbitals and require the convergence of our observables, like the one- and two-body density matrix, with respect to the number of single-particle states M.

A set of coupled equations of motion for, both, the time-dependent expansion coefficients $C_{\vec{n}}(t)$ and the time-dependent orbitals $\phi_k(x, t)$ are obtained by requiring the stationarity of the action of the time-dependent

Schrödinger equation[43,44] under variations of $C_{\vec{n}}(t)$ and $\phi_k(x, t)$. Using MCTDHB, both, the coefficients and orbitals are variationally optimized[64]. MCTDHB is thus fundamentally different from exact diagonalization, i.e., an ansatz built with *time-independent* orbitals. It can be demonstrated that MCTDHB delivers solutions of the Schrödinger equation at a significantly increased accuracy in comparison to exact diagonalization approaches when the same number of single-particle basis states is employed, see Refs.[53,65]. for a demonstration with the harmonic interaction model and Appendix A for a demonstration with dipole-dipole interactions, i.e., the Hamiltonian in Eqs. (2) and (4). Despite the accuracy of MCTDHB for weakly interacting particles, for strong interactions a large number of orbitals is required to describe the system accurately. In the case $\lambda \to \infty$, the Bose-Fermi mapping provides analytical solutions that can be compared to the numerical results. These difficulties to converge MCTDHB results for strong contact interactions may be an instance of the discussion provided in Ref.[66].

We solve the set of coupled MCTDHB equations using the MCTDH-X software[46,52–54]. When imaginary time is used, the propagation of an initial guess function converges to the ground state of the system, and the stationary properties of the system can be investigated.

Fermionization vs Crystallization

We now discuss our findings on the fermionized and the crystalline state of parabolically trapped one-dimensional ultracold bosons. We first independently characterize fermionization and crystallization from a "many-body point of view", see Sec. 4.1 and Sec. 4.2, respectively. Thereafter, we investigate how to sort the one, fermionization, from the other, crystallization, in Sec. 4.3. Here and in the following, we used the term "many-body point of view" to highlight that our considerations go beyond an effective single-particle or mean-field description of the state.

Fermionization. Bosons fermionize when they feel an infinitely repulsive contact interaction in one spatial dimension. For fermionized bosons, the total energy E and the density [Eq. (6)] of the system become exactly equal to the energy and the density of non-interacting spinless fermions, respectively. For our showcase of few-bosons systems (N = 2 to N = 5) in a harmonic trap with frequency one, $V(x) = \frac{1}{2}x^2$, the limiting value is thus $E^N_{\lambda\to\infty} = \frac{N^2}{2}$.

We start our investigation with the one-body density as a function of the interaction strength λ [Fig. 1(a–b)]. For comparatively weak repulsion, the density is clustered at the center of the trap, but becomes flatter and broader when λ increases. For stronger repulsion, the density gradually acquires modulations and the number of humps finally saturates to the number of bosons in the system; four humps for $N = 4$ bosons are clearly visible when the interaction strength goes above $\lambda \sim 10$. The emergence of N maxima in the density indicates that the TG regime is approached. The density modulations/humps are more pronounced in the center of the trap, where the potential is close to zero. For larger distances from the origin, the humps in the density are less pronounced due to the non-zero value of the confinement potential. Importantly, the outermost density modulation also becomes less pronounced if the number of particles N is increased. See also Appendix B for a direct comparison of the relative height of innermost and outermost peaks for different particle numbers N.

We note that the density's maxima in the Tonks-Girardeau regime are distinct but *not isolated*. We also observe that, once the TG regime is reached, the density does not broaden further with increasing values of λ for all particle numbers. We also provide a direct comparison with the ground state properties of non-interacting fermions computed with the multiconfigurational time-dependent Hartree method for fermions (MCTDHF), see Fig. 2. We note that the results for non-interacting fermions can be obtained analytically, i.e., here, we use the heavy MCTDHF method only for the sake of computational convenience.

We now move to discuss the two-body densities $\rho^{(2)}$ of bosons with contact interactions [see Fig. 3(a)]. For weak interaction strength, $\lambda = 0.1$, the bosons are clustered near the center, i.e, at $x_1 = x_2 = 0$ [Fig. 3(a)]. As the interaction strength increases, $\rho^{(2)}$ spreads out to the off-diagonal ($x_1 \neq x_2$) while the diagonal ($x_1 \sim x_2$) is depleted [see Fig. 3(a) for $\lambda = 1$].

For stronger repulsion a so-called "correlation hole" in the two-body density forms on the diagonal, $\rho^{(2)}(x, x) \to 0$ [see Fig. 3(a) for $\lambda = 10$ and $\lambda = 30$]. The probability of finding two bosons at the same position tends towards zero. In the limit of infinite repulsion the correlation hole persists in $\rho^{(2)}$. In analogy, however, to the boundedness of the energy as a function of the interaction strength, the width of two-body density on its anti-diagonal $[\rho^{(2)}(x, -x)]$ is also bounded, i.e., the spread of $\rho^{(2)}$ converges in the fermionization limit when $\lambda \to \infty$.

Similar to the one-body density, the maxima which are formed in the off-diagonal of the two-body density are distinct but not isolated [see Fig. 3(a) for $\lambda = 10$ and $\lambda = 30$].

We infer that *the correlation hole along the diagonal* and *the confined spread* are the unique signatures of the two-body density of a fermionized state.

Crystallization. For bosons with dipole-dipole interactions, crystallization occurs when the long-range tail of the interaction [see Eq. (4)] becomes dominant[34]: the bosons form a lattice structure which allows them to minimize their mutual overlap. To characterize crystallization we analyze the one-body and two-body density for bosons with dipolar interaction of strength g_d. We choose the cut-off parameter $\alpha = 0.05$ in Eq. (4) such that the effective interaction features the same physical beahavior as the "real" dipolar interaction that additionally contains a contact-interaction term (see Ref.[34] for a direct comparison).

We plot the one-body density of $N = 4$ bosons as a function of g_d in Fig. 1(c,d). The system is condensed at the center of the trap for small g_d. As g_d increases, the density starts to exhibit a four-hump structure (see Fig. 1(c,d) for $g_d \in [\sim 1, \sim 5]$) similar to the density observed for the fermionization of bosons with contact interactions [Fig. 1(a)].

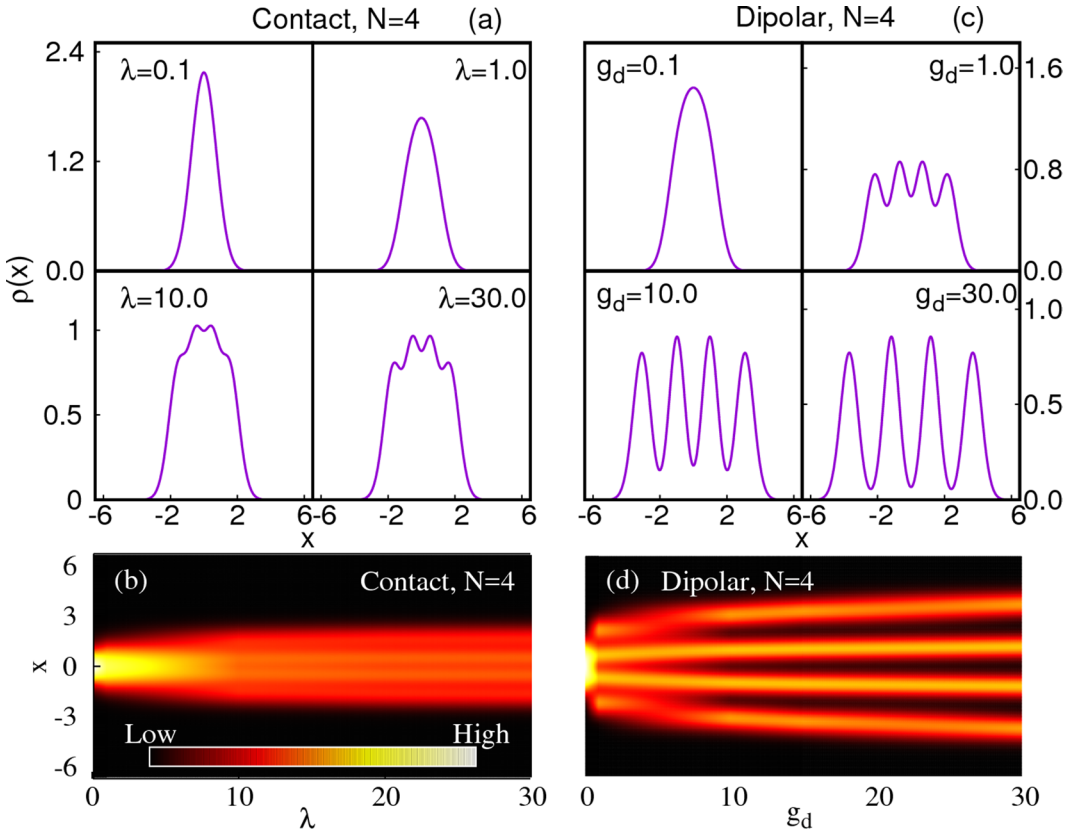

Figure 1. One-body density of N = 4 bosons as a function of contact [(**a**,**b**)] and dipolar [(**c**,**d**)] interparticle interaction strength. *For contact interactions*, the density becomes flatter and broader as the repulsion increases [panel **(a)** and **(b)** for $\lambda \leq 1$]. For even larger interaction strengths [panel **(a)** and **(b)** for $\lambda \gtrsim 10$], four distinct but not isolated peaks appear and the density gradually converges to the density of four non-interacting fermions as $\lambda \to \infty$. Due to this convergence, the spread of the density seizes to increase [panel **(d)**]. *For dipolar interactions*, the one-body density is clustered at the center of the trap for small interactions [panels (c,d) for $g_d \lesssim 1$]. As g_d increases, the density develops a fourfold splitting [panel **(c)** and **(d)** for $g_d \gtrsim 1$]. As a function of increasing interaction strength, the spread of the density continues to increase [panel **(d)**] and the fourfold spatial splitting intensifies to form four almost completely isolated peaks in the density for sufficiently strong dipolar interactions: crystallization emerges [panels **(c,d)** for $g_d \gtrsim 10$]. All quantities shown are dimensionless.

This *attempted fermionization* results from a dominant contribution of the short-range part of the dipolar interaction potential, see also Ref.[18]. However, this fermionization-like behavior is only a precursor to the crystal transition that takes place when the long-range nature of the interaction starts to dominate the physics of the system for larger interaction strengths [Fig. 1(c,d) for $g_d \gtrsim 10$]. For crystallized dipolar bosons at sufficiently large g_d, the value of the density at its minima between the humps tends to zero while the spreading of the density profile diverges as g_d increases, see Fig. 4. At $g_d = 30.0$, we observe four *well-isolated* peaks heralding the crystallization of the $N = 4$ bosons. We collect results for other numbers of bosons ($N = 2, 3, 5, 6$) with dipole-dipole interactions – including the relative height of the peaks in the density that shows that the peaks are well-isolated in comparison to particles with contact interactions – in Appendix B. A comparison of MCTDHB results with exact diagonalization is shown in Appendix A.

We now analyze the two-body density for dipole-dipole interactions [Fig. 3(b)]. For small interaction strength, $g_d = 0.1$, the atoms are clustered together at the center of the trap. As g_d increases, a correlation hole develops: $\rho^{(2)}(x, x)$ tends to zero [Fig. 3(b) for $g_d \geq 1$]. Thus, due to the long-range interaction, the probability of finding two bosons in the same place is strongly reduced. In the crystalline phase [Fig. 3(b) for $g_d \geq 10$]: the bosons escape their spatial overlap entirely and even the off-diagonal peaks of $\rho^{(2)}$ become isolated. We term this behavior the formation of an off-diagonal correlation hole. For crystallized bosons, the spread of the anti-diagonal of the two-body density, $\rho^{(2)}(x, -x)$, is diverging as g_d is increasing [compare Fig. 3(b) for $g_d = 10$ to Fig. 3(b) for $g_d = 30$].

We assert that *the correlation hole along the diagonal and the off-diagonal* and *the unbounded spreading* are the unique signatures of the two-body density of a crystalline state of dipolar bosons.

Sorting crystallization from fermionization. We now discuss how to distinguish fermionized from crystallized many-body states. One clear distinction is given by the spread of the one- and two-body densities: for bosons with contact interactions it is bounded, while for bosons with dipole-dipole interactions it diverges as a function of the interaction strength. We assert that, **(1)** the bounded spreading of the density for contact

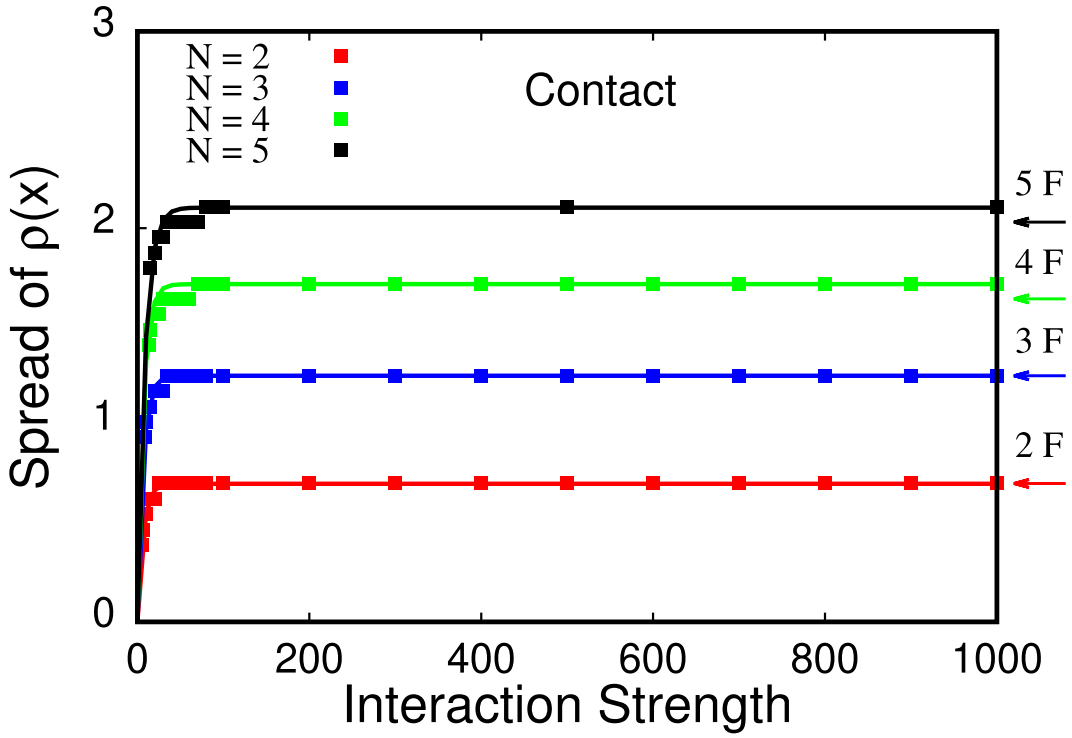

Figure 2. Spread of the density $\rho(x)$ as a function of the interaction strength for $N=2, 3, 4, 5$ (bottom to top curve, respectively) bosons with contact interparticle interactions. The spread of the density, according to the fitted curves (solid lines) converges exponentially as $A_N[\exp(-\lambda/B_N)-1]$ to the fermionization limit as $\lambda\to\infty$ which is shown by the arrows labeled "2F", "3F", "4F", "5F" on the right hand side of the plot. The fit parameters for $N=2, 3, 4, 5$ are, respectively, $(A_2=-0.701491, B_2=6.45191)$, $(A_3=-1.25018, B_3=6.50518)$, $(A_4=-1.71554, B_4=6.8185)$, $(A_5=-2.10423, B_5=8.63662)$. All quantities shown are dimensionless.

interactions is a consequence of the bounded energy as the interaction strength tends to infinity. Similarly, we assert, **(2)** that the unbounded spreading of the density for dipole-dipole interactions is a consequence of the unbounded energy as the interaction strength g_d tends to infinity. To validate the assertions **(1)** & **(2)**, we quantify the spreading of the density as a function of interactions and plot the position of its outermost peak as a function of the interaction strength in Fig. 5(a) and compare it to the energy in Fig. 5(b), for $N=4$.

From fitting the energy in Fig. 5(b) we can infer that the energy as a function of contact interaction strength approaches the fermionization limit exponentially, a power law does not fit as accurately the data. For very large interactions, in the limit of $\lambda^{-1}\to 0$, our results are in agreement with the analysis in Ref.[67], see Appendix B. For dipolar interactions, the growth of the energy as a function of the interaction strength is fitting well to a power law.

Indeed, the comparison of Fig. 5(a,b) corroborates our assertions **(1)** & **(2)**, and holds for different number of particles.

We thus conclude that the crystalline phase can be distinguished from the TG regime gas by virtue of the behavior of its density profile as a function of the strength of the interparticle interactions: The width of the density distribution *converges* for an increasing strength of contact interactions, but it *continuously spreads* for an increasing strength of long-range interactions [compare Fig. 1(b) with Fig. 1(d) as well as Fig. 5(a) with Fig. 5(b)]. In Appendix B, we demonstrate that the exponent of the power law of the spreading of the density as a function of the strength of the interaction is independent of the particle number N.

In the case of long-ranged interactions, the unbounded spreading of densities as a function of increasing interaction strength and the formation of well-isolated peaks are in sharp contrast to the bounded spreading of densities and the non-isolated peaks in the case of contact interactions in the TG regime [cf. Figs 1 and 5(a–b)].

We now turn to analyze the eigenvalues of the reduced one-body density matrix, the so-called natural occupations[60], as a function of the interaction strength between the particles [Fig. 5(c,d)]. As expected[8,33,34], when the value of the interaction strength increases, the occupation of the first natural orbital decreases while the other orbitals start to be occupied. For contact interactions, mostly one natural occupation, n_1, dominates, while the other occupations n_k, $k>1$ remain comparatively small even for large values of λ: depletion emerges as the fermionized state is reached [Fig. 5(c)], see also Ref.[8]. For long-range interactions, however, all occupations $\rho_k^{(NO)}$ for $k\leq N$ contribute on an equal footing for large values of g_d. This full-blown N-fold fragmentation emerges as the crystal state is reached [Fig. 5(d)], see also Ref.[34]. In the crystal state the bosons behave similar to distinguishable particles[68], and the particle statistics does not influence the physical observables considered in Fig. 5(b,d): the

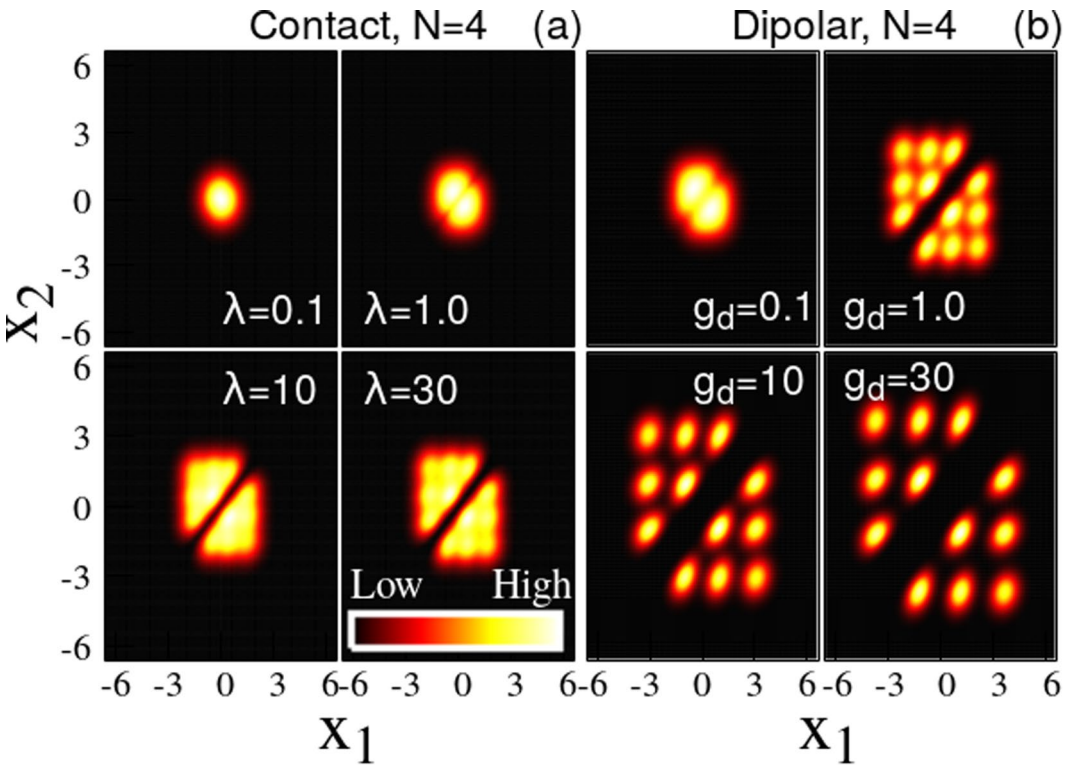

Figure 3. Two-body density of N = 4 bosons as a function of contact **(a)** and dipolar [**(b)**] interparticle interaction strength. *For contact interactions*, the atoms are clustered at the center ($x_1 = x_2 = 0$) for small interaction strengths, [panel **(a)** for $\lambda = 0.1$]. As λ increases, the two-body density starts to spread due to the repulsion between the bosons [panel **(a)** for $\lambda = 1$]. For stronger interaction strengths, $\lambda = 10$ and $\lambda = 30$ in (**a**), the diagonal, $\rho^{(2)}(x, x)$, is practically 0: the bosons completely avoid to be at the same position and a "correlation hole" develops. *For dipolar interactions*, the atoms cluster at the center ($x_1 = x_2 = 0$) for small interaction strengths, see panel **(b)** for $g_d = 0.1$. As g_d increases, the diagonal part, $\rho^{(2)}(x, x)$ starts to be depleted because the long-range interactions start to dominate the physics [panel **(b)** for $\gtrsim 1$]. At stronger interaction strengths, the diagonal correlation hole spreads, i.e., the area in the vicinity of $x_1 \approx x_2$ for which $\rho^{(2)}(x_1, x_2) \approx 0$ holds is enlarged as a function of g_d [compare panel **(b)** for $g_d = 1.0$, 10, and 30]. In contrast to contact interactions, even the off-diagonal ($x_1 \neq x_2$) of $\rho^{(2)}(x_1, x_2)$ forms a complete correlation hole, compare panel **(a)** for $\lambda = 30$ and panel **(b)** for $g_d = 30$. All quantities shown are dimensionless.

energy and the natural occupations for bosons and fermions converge to the same values. Thus, the finding of Ref.[68] for two particles may be extended to larger number of particles.

The emergence of complete fragmentation is a consequence of long-ranged interactions and in sharp contrast to the emergent depletion in the case of contact interactions.

Conclusions

In this paper we highlight the key characteristics of the many-body wavefunction that reveal the difference between the fermionized bosons with contact interactions and crystallized bosons with dipolar interactions.

In the case of fermionization, the one-(two-)body density shows a modulation with a number of maxima corresponding to the number of particles. The maxima are confined but not completely separated. The incomplete separation is a consequence of the representability of momentum distribution of fermionized bosons using a basis set: infinitely many basis states are necessary to accurately resolve the cusp – a fact that is reflected by the depletion of the state which we quantified by the eigenvalues of the reduced one-body density matrix. We found that the peaks in the density as well as the energy as a function of the interaction strength approach the fermionization limit exponentially.

In the case of crystallization, the one-(two-)body density shows well-separated peaks whose distances diverge as a function of the interaction strength as a power law. This completed separation is the consequence of the formation of a Mott-insulator-alike many-body state where the "lattice potential" is replaced by the long-ranged interparticle interactions and the "lattice constant" is dictated by the strength of the interparticle interactions.

We close by stating that all the signatures that distinguish crystalline bosons from fermionized bosons can be measured experimentally using single-shot absorption imaging[69–73]. From experimental absorption images, the one-body and two-body density are available as averages of many single-shot images. Thus, a direct verification of our results for the spread of the one-body and two-body density can be performed. Furthermore, Refs.[34,63] suggest that the natural occupations can be inferred from the integrated variance of single-shot images, at least at zero

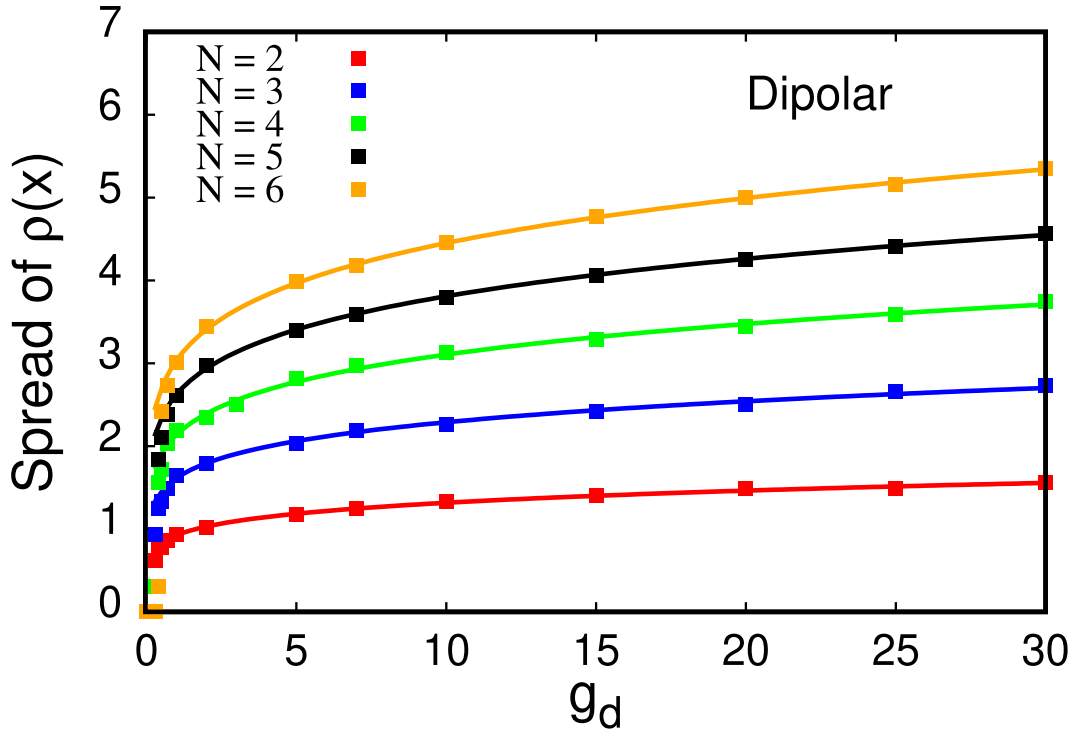

Figure 4. Spread of the density for $N = 2, 3, 4, 5, 6$ bosons (bottom to top curve, respectively) with dipole-dipole interactions as a function of the interaction strength g_d. The spread of the density, according to the fitted curves (solid lines) diverges as a power law, $C_N x^{D_N}$, in the limit of large interactions $g_d \to \infty$. The fit parameters for $N = 2, 3, 4, 5, 6$ are, respectively, ($C_2 = 0.926851$, $D_2 = 0.152459$), ($C_3 = 1.61556$, $D_3 = 0.151243$), ($C_4 = 2.13826$, $D_4 = 0.162034$), ($C_5 = 2.62615$, $D_5 = 0.161553$), ($C_6 = 3.03802$, $D_6 = 0.165883$). Importantly, the power of the divergence of the spread, D_N, seems to be independent of the number of particles N. All quantities shown are dimensionless.

temperature. It is, of course, an open question how thermal fluctuations affect the variance in absorption images and up to which temperature it is still possible to determine the fragmentation of the system.

Appendix A: Comparison of MCTDHB and exact diagonalization

In this Appendix, we demonstrate that MCTDHB yields solutions to the Schrödinger equation at a larger accuracy as compared to the exact diagonalization approach (ED). As is conventional, we use the eigenfunctions of the non-interacting system as the single-particle basis states for the ED. We solve the same system as shown in Fig. 1(c),(d) for an interaction strength of $g_d = 30$ and compare the energies obtained with MCTDHB and ED, see Fig. 6. Due to the variationally optimized single-particle basis in MCTDHB computations it features a much smaller error than the ED computations with an unoptimized single-particle basis for the same number of orbitals. This observation is in agreement with other works that benchmark the MCTDHB and the MCTDHF approaches against ED, see Ref.[65] and Ref.[46], respectively.

Appendix B: Different Particle Numbers

In this Appendix, we corroborate our results in the main text by studying different particle numbers.

Contact interactions. The results of the manuscript have been obtained with MCTDHB with $M = 12, 14, 20, 22$ orbitals for $N = 2, 3, 4, 5$ bosons, respectively, with a contact interaction strength up to $\lambda = 1000$. In Fig. 2 of the main text, our results are consistent with fits of an exponential function $A_N[exp(-\lambda/B_N) - 1]$, see caption of Fig. 2 for the fitting parameters A_N and B_N. Furthermore, we assess the convergence of the spread of the density as a function of the interaction strength to the spread of the density of the non-interacting fermionic system, see arrows labeled "2F","3F","4F", and "5F" in Fig. 2.

To compare our results for the energy in the fermionization limit to analytical predictions for very large contact interaction strengths in Ref.[67], we plot the energies as a function of $-\lambda^{-1}$ in Fig. 7. We find that our results are consistent with the linear limit for the energy as a function of $-\lambda^{-1}$ of Ref.[67].

We now turn to the relative height of the innermost and outermost peak(s),

$$\Delta\rho(x) = \frac{\rho_{\max} - \rho_{\min}}{\rho_{\max} + \rho_{\min}} \tag{B1}$$

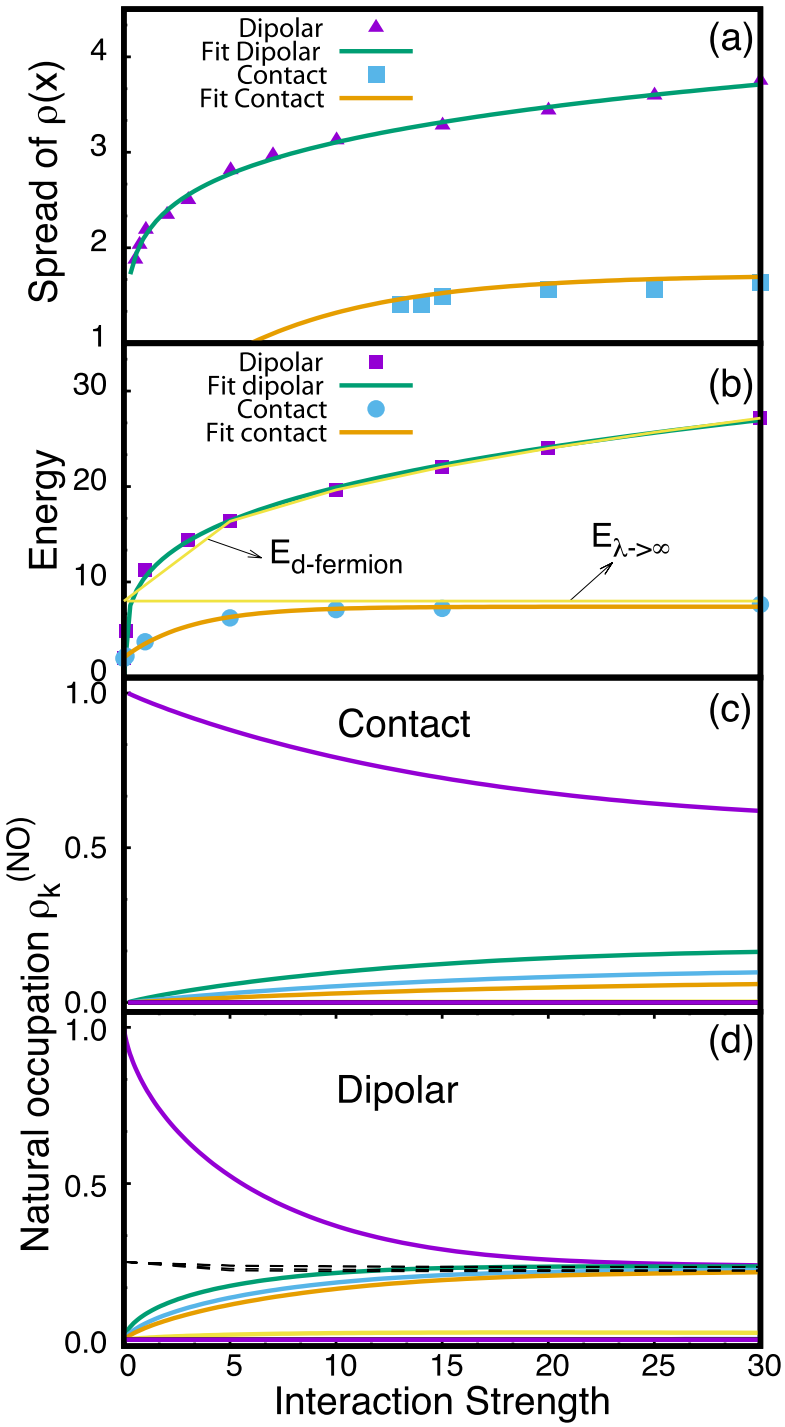

Figure 5. Tracing fermionization and crystallization in the spread of the density (**a**), the energy (**b**), and the natural occupations (**c**,**d**) as a function of the interaction strength. (**a**) The spread of the density is quantified by the position of the outermost peak in the density $\rho(x)$. The spread is bounded for contact interactions and unbounded for dipolar interactions. The fits shown suggest that the spread of the density $\rho(x)$ for dipolar interactions diverges with a power law, $2.138 g_d^{0.162}$, and for contact interactions it converges as $-1.71554[\exp(-\lambda/6.8185)-1]$ to the fermionization limit (fit obtained with more points than actually shown, see Appendix 7). (**b**) The energy as a function of interaction strength is bounded for contact interactions and unbounded for dipolar interactions. The fits suggest that the energy diverges with a power law $10.51 g_d^{0.277}$ for dipolar interactions and converges to the fermionization limit exponentially $-5.84\exp(-\lambda/6.023)+8.133$ for contact interactions. The thin yellow lines indicate the energy of non-interaction fermions $E_{\lambda\to\infty}$ and the energy for dipolar fermions $E_{d-fermion}$. (**c**,**d**) The eigenvalues of the reduced density matrix, i.e., the natural occupations $\rho_i^{(NO)}$, exhibit depletion for contact interactions (many small $\rho_i^{(NO)}$ with $i>1$ emerge) and full-blown N-fold fragmentation for dipolar interactions (all $\rho_i^{(NO)}$ with $i\leq N$ contribute equally), the black dashed lines show the four most populated natural orbitals for dipolar fermions. The $\rho_i^{(NO)}$ are ordered in decreasing order starting from $i=1$. All quantities shown are dimensionless.

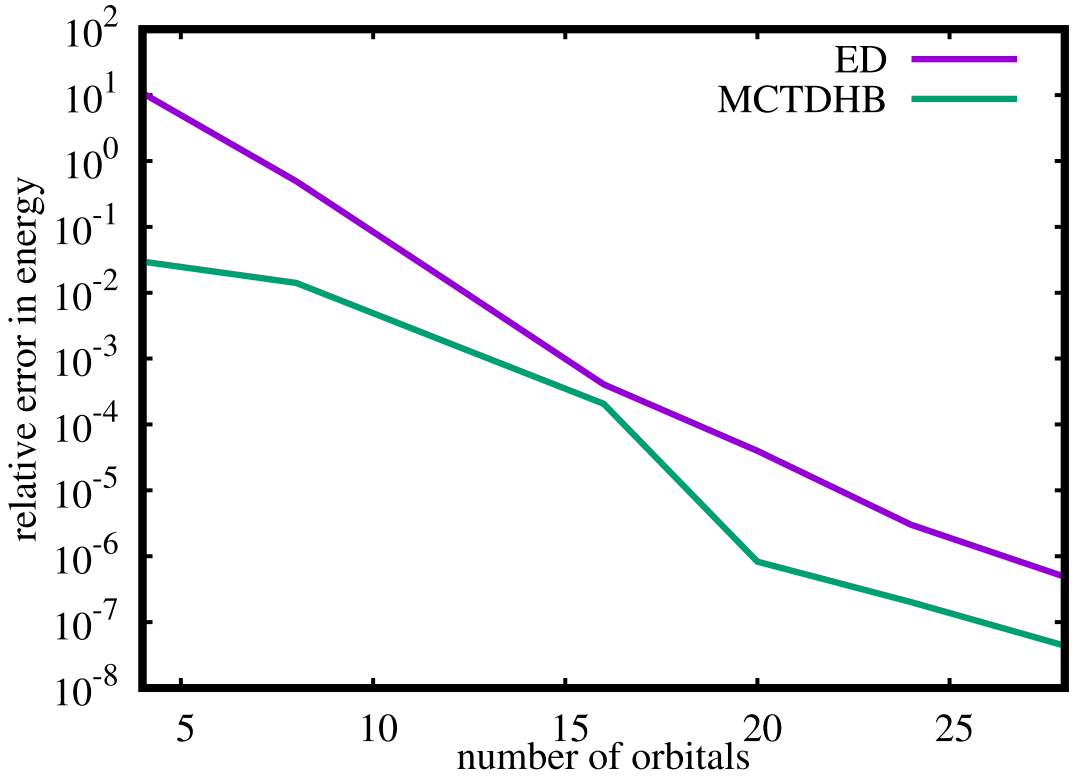

Figure 6. Comparison of MCTDHB and ED for $N = 4$ bosons with dipole-dipole interaction strength $g_d = 30$. The plot shows the relative error in energy with respect to an MCTDHB computation with $M = 32$ orbitals as a function of the number of orbitals for the ED and MCTDHB approaches. Due to the variationally optimized basis in MCTDHB computations it features a much smaller error for any number of orbitals. All quantities shown are dimensionless.

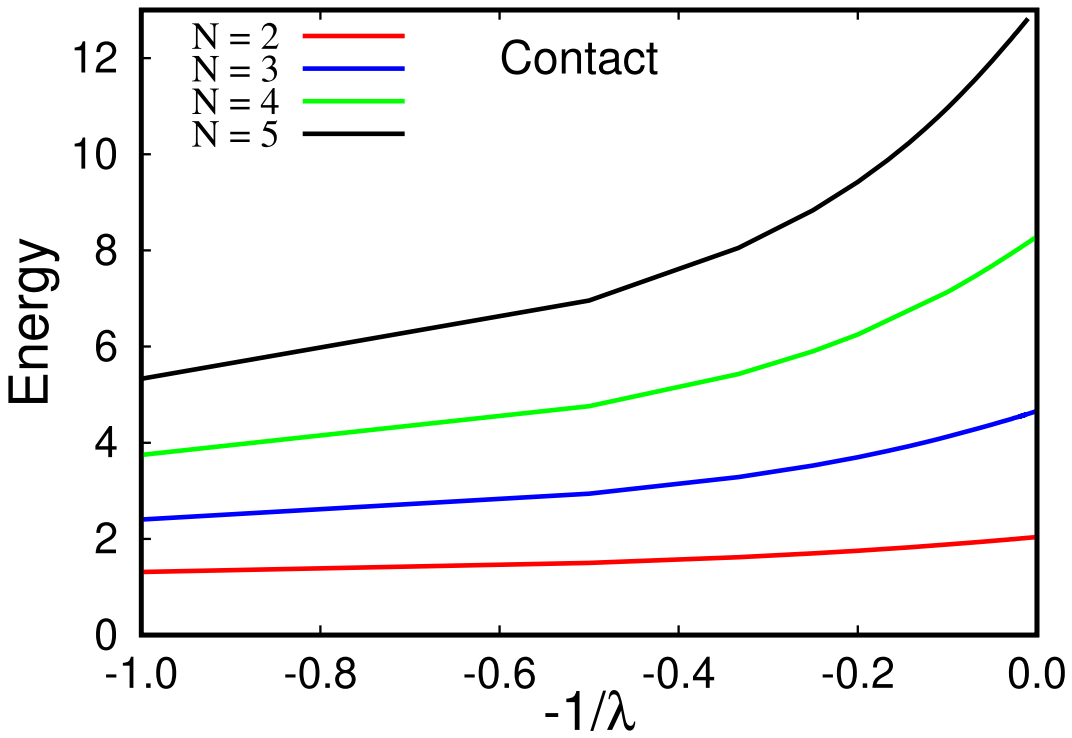

Figure 7. Energy as a function of inverse interaction strength, $-1/\lambda$, for $N = 2, 3, 4, 5$ (bottom to top curve, respectively) bosons. Our results are consistent with the analysis in Ref.[67]: the energy linearly converges to the fermionization limit, i.e., when $-\lambda^{-1} \to 0$. All quantities shown are dimensionless.

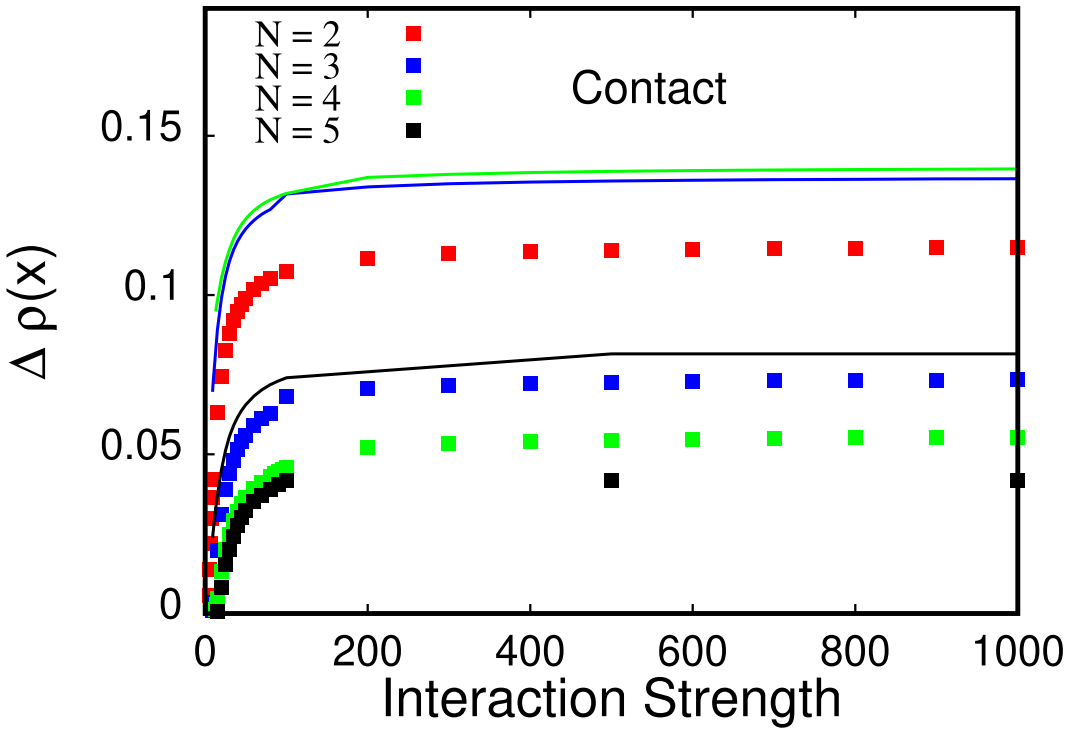

Figure 8. Relative height of the outermost peaks in the density of $N = 2, 3, 4, 5$ bosons with contact interactions (points, top to bottom, respectively) and relative height of the innermost peaks in the density of $N = 4, 3, 5$ bosons with contact interactions (lines, top, to bottom, respectively). The relative peak height is consistently smaller for the outermost peak as compared to the innermost peak in the density for all interaction strengths depicted. All quantities shown are dimensionless.

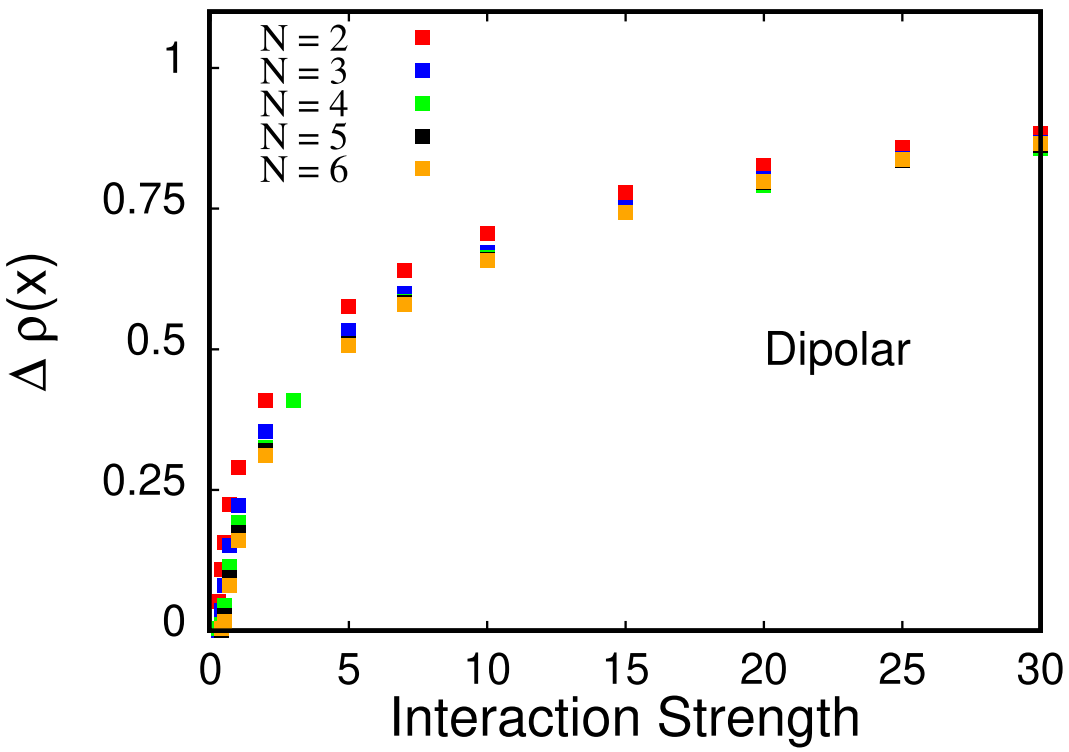

Figure 9. Relative peak height for $N = 2, 3, 4, 5, 6$ bosons with dipolar interactions as a function of interaction strength. The relative peak height converges towards unity similarly for all particle numbers investigated here as the interaction strength increases. All quantities shown are dimensionless.

in the density. Here, ρ_{max} refers to the value of the density $\rho(x)$ at the peak position and ρ_{min} refers to the value of the density $\rho(x)$ at the position of the minimum to the left to the considered peak. See Fig. 8 for a plot of $\Delta\rho(x)$ for $N=2, 3, 4, 5$ bosons. It is clearly seen that, for fixed N, the outermost peaks' relative height is much smaller than the relative height of the innermost peaks.

Dipolar interactions. Here, we assess the validity of the power-law-like unbounded spreading of the density as a function of the strength of dipole-dipole interactions, that we have shown in Fig. 4 of the main text for $N=4$ particles. In Fig. 4 We plot the spread of the density for $N=2, 3, 4, 5, 6$ dipolar bosons obtained with MCTDHB with $M=16, 16, 22, 28, 26$ orbitals, respectively, and fit it with a power law $C_N g_x^{D_N}$. We find that the exponent in the power law is almost identical for all particle numbers studied here, i.e., $D_N \approx 0.16$ for $N=2, 3, 4, 5, 6$.

We now discuss the relative peak height $\Delta\rho(x)$, see Eq. (B1), of the outermost peak as a function of the dipolar interaction strength, see Fig. 9 for a plot for $N=2, 3, 4, 5, 6$. As hinted by Fig. 1(c) in the main text, the relative peak height for the case of the dipole-dipole interactions converges towards unity as the strength of interactions g_d increases, because the values of the minimum, ρ_{min} in Eq. (B1), tends to zero: the peaks in the crystal state are *well-isolated* in comparison to the peaks in the fermionization limit for bosons with contact interactions (compare magnitude of relative peak heights in Figs. 8 and 9).

Received: 26 April 2019; Accepted: 23 October 2019;
Published online: 29 November 2019

References

1. Petrov, D. S., Shlyapnikov, G. V. & Walraven, J. T. M. Regimes of Quantum Degeneracy in Trapped 1D Gases. *Phys. Rev. Lett.* **85**, 3745 (2000).
2. Dunjko, V., Lorent, V. & Olshanii, M. Bosons in Cigar-Shaped Traps: Thomas-Fermi Regime, Tonks-Girardeau Regime, and In Between. *Phys. Rev. Lett.* **86**, 5413 (2001).
3. Görlitz, A. *et al*. Realization of Bose-Einstein Condensates in Lower Dimensions. *Phys. Rev. Lett.* **87**, 130402 (2001).
4. Greiner, M. *et al*. Exploring Phase Coherence in a 2D Lattice of Bose-Einstein Condensates. *Phys. Rev. Lett.* **87**, 160405 (2001).
5. Zürn, G. *et al*. Fermionization of Two Distinguishable Fermions. *Phys. Rev. Lett.* **108**, 075303 (2012).
6. Jacqmin, T., Armijo, J., Berrada, T., Kheruntsyan, K. V. & Bouchoule, I. Sub-Poissonian Fluctuations in a 1D Bose Gas: From the Quantum Quasicondensate to the Strongly Interacting Regime. *Phys. Rev. Lett.* **106**, 230405 (2011).
7. Girardeau, M. Relationship between Systems of Impenetrable Bosons and Fermions in One Dimension. *J. Math Phys* **1**, 516 (1960).
8. Zöllner, S., Meyer, H.-D. & Schmelcher, P. Correlations in ultracold trapped few-boson systems: Transition from condensation to fermionization. *Phys. Rev. A* **74**, 063611 (2006).
9. Alon, O. E. & Cederbaum, L. S. Pathway from Condensation via Fragmentation to Fermionization of Cold Bosonic Systems. *Phys. Rev. Lett.* **95**, 140402 (2005).
10. Zöllner, S., Meyer, H.-D. & Schmelcher, P. Composite fermionization of one-dimensional Bose-Bose mixtures. *Phys. Rev. A* **78**, 013629 (2008).
11. Roy, R. *et al*. Phases, many-body entropy measures, and coherence of interacting bosons in optical lattices. *Phys. Rev. A* **97**, 043625 (2018).
12. Kościk, P. Fermionized Dipolar Bosons Trapped in a Harmonic Trap. *Few-Body Syst* **58**, 59 (2017).
13. Arkhipov, A. S., Astrakharchik, G. E., Belikov, A. V. & Lozovik, Y. E. Ground-state properties of a one-dimensional system of dipoles. *JETP Lett* **82**, 39 (2005).
14. Zöllner, S., Bruun, G. M., Pethick, C. J. & Reimann, S. M. Bosonic and Fermionic Dipoles on a Ring. *Phys. Rev. Lett.* **107**, 035301 (2011).
15. Zöllner, S. Bosonic and Fermionic Dipoles on a Ring. Ground states of dipolar gases in quasi-one-dimensional ring traps. *Phys. Rev. A* **84**, 063619 (2011).
16. Astrakharchik, G. E., Morigi, G. E., De Chiara, G. & Boronat, J. Ground state of low-dimensional dipolar gases: Linear and zigzag chains. *Phys. Rev. A* **78**, 063622 (2008).
17. Astrakharchik, G. E. & Lozovik, Y. E. Super-Tonks-Girardeau regime in trapped one-dimensional dipolar gases. *Phys. Rev. A* **77**, 013404 (2008).
18. Deuretzbacher, F., Cremon, J. C. & Reimann, S. M. Ground-state properties of few dipolar bosons in a quasi-one-dimensional harmonic trap. *Phys. Rev. A* **81**, 063616 (2010).
19. Sowiński, T. & García-March, M. Á. One-dimensional mixtures of several ultracold atoms: a review. *Rep. Prog. Phys.* **82**, 104401 (2019).
20. Paredes, B. *et al*. Tonks–Girardeau gas of ultracold atoms in an optical lattice. *Nature* **429**, 277 (2004).
21. Deuretzbacher, F. *et al*. Evolution from a Bose-Einstein condensate to a Tonks-Girardeau gas: An exact diagonalization study. *Phys. Rev. A* **75**, 013614 (2007).
22. Kinoshita, T., Wenger, T. & Weiss, D. S. Observation of a One-Dimensional Tonks-Girardeau Gas. *Science* **305**, 1125 (2004).
23. Santos, L., Shlyapnikov, G. V. & Lewenstein, M. Roton-Maxon Spectrum and Stability of Trapped Dipolar Bose-Einstein Condensates. *Phys. Rev. Lett.* **90**, 250403 (2003).
24. Andre, A. *et al*. A coherent all-electrical interface between polar molecules and mesoscopic superconducting resonators. *Nature Phys* **2**, 636 (2006).
25. Büchler, H. P. *et al*. Strongly Correlated 2D Quantum Phases with Cold Polar Molecules: Controlling the Shape of the Interaction Potential. *Phys. Rev. Lett.* **98**, 060404 (2007).
26. Baranov, M. A. Theoretical progress in many-body physics with ultracold dipolar gases. *Phys. Rep* **464**, 71 (2008).
27. Griesmaier, A., Werner, J., Hensler, S., Stuhler, J. & Pfau, T. Bose-Einstein Condensation of Chromium. *Phys. Rev. Lett.* **94**, 160401 (2005).
28. Beaufils, Q. *et al*. All-optical production of chromium Bose-Einstein condensates. *Phys. Rev. A* **77**, 061601 (2008).
29. Lahaye, T., Menotti, C., Santos, L., Lewenstein, M. & Pfau, T. The physics of dipolar bosonic quantum gases. *Rep. Prog. Phys.* **72**, 126401 (2009).
30. Romanovsky, I., Yannouleas, C. & Landman, U. Crystalline Boson Phases in Harmonic Traps: Beyond the Gross-Pitaevskii Mean Field. *Phys. Rev. Lett.* **93**, 230405 (2004).
31. Kościk, P. Quantum correlations in one-dimensional Wigner molecules. *Eur. Phys J. D* **71**, 286 (2017).
32. Kościk, P. The von Neumann entanglement entropy for Wigner-crystal states in one dimensional N-particle systems. *Phys. Lett. A* **379**, 293 (2015).
33. Chatterjee, B., Brouzos, I., Cao, L. & Schmelcher, P. Ultracold dipolar few-boson ensembles in a triple-well trap. *J. Phys. B: At. Mol. Opt. Phys* **46**, 085304 (2013).

34. Chatterjee, B. & Lode, A. U. Order parameter and detection for a finite ensemble of crystallized one-dimensional dipolar bosons in optical lattices. *J. Phys. Rev. A* **98**, 053624 (2018).
35. Wigner, E. On the Interaction of Electrons in Metals. *Phys. Rev* **46**, 1002 (1934).
36. Aikawa, K. *et al*. Bose-Einstein Condensation of Erbium. *Phys. Rev. Lett.* **108**, 210401 (2012).
37. Frisch, A. *et al*. Ultracold Dipolar Molecules Composed of Strongly Magnetic Atoms. *Phys. Rev. Lett.* **115**, 203201 (2015).
38. Park, J. W., Will, S. A. & Zwierlein, M. W. Ultracold Dipolar Gas of Fermionic 23Na40K Molecules in Their Absolute Ground State. *Phys. Rev. Lett.* **114**, 205302 (2015).
39. Xu, Z., Li, L., Xianlong, G. & Chen, S. Wigner crystal versus fermionization for one-dimensional Hubbard models with and without long-range interactions. *J. Phys.: Condens. Matter* **25**, 055601 (2013).
40. Pethick, C. J. & Smith, H. *Bose-Einstein Condensation in Dilute Gases* (Cambridge University Press, Cambridge UK, 2002).
41. Bogoliubov, N. N., *Selected Works II: Quantum and Statistical Mechanics* (Gordon and Breach, New York, 1991).
42. Pitaevskii, L. P. & Stringari, S., *Bose-Einstein Condensation* (Clarendon Press, Oxford, 2003).
43. Alon, O. E., Streltsov, A. I. & Cederbaum, L. S. Multiconfigurational time-dependent Hartree method for bosons: Many-body dynamics of bosonic systems. *Phys. Rev. A* **77**, 033613 (2008).
44. Streltsov, A. I., Alon, O. E. & Cederbaum, L. S. Role of Excited States in the Splitting of a Trapped Interacting Bose-Einstein Condensate by a Time-Dependent Barrier. *Phys. Rev. Lett.* **99**, 030402 (2007).
45. Cao, L., Krönke, S., Vendrell, O. & Schmelcher, P. The multi-layer multi-configuration time-dependent Hartree method for bosons: Theory, implementation, and applications. *J. Chem. Phys.* **139**, 134103 (2013).
46. Fasshauer, E. & Lode, A. U. Multiconfigurational time-dependent Hartree method for fermions: Implementation, exactness, and few-fermion tunneling to open space. *J. Phys. Rev. A* **93**, 033635 (2016).
47. Léveque, C. & Madsen, L. B. Time-dependent restricted-active-space self-consistent-field theory for bosonic many-body systems. *New Journal of Physics* **19**, 043007 (2017).
48. Léveque, C. & Madsen, L. B. Multispecies time-dependent restricted-active-space self-consistent-field theory for ultracold atomic and molecular gases. *Journal of Physics B* **51**, 155302 (2018).
49. Lode, A. U. J., Léveque, C., Madsen, L. B., Streltsov, A. I. & Alon, O. E. Multiconfigurational time-dependent Hartree approaches for indistinguishable particles, *arXiv:1908.03578*.
50. Mese, A. I., Capuzzi, P., Aktas, S., Akdeniz, Z. & Okan, S. E. Condensation of two-dimensional harmonically confined bosons with Bessel-type interactions. *Phys. Rev. A* **84**, 043604 (2011).
51. Yannouleas, C. & Landman, U. Symmetry breaking and quantum correlations infinite systems: studies of quantum dots andultracold Bose gases and related nuclear andchemical methods. *Rep. Prog. Phys.* **70**, 2067 (2007).
52. Lode, A. U. J. *et al*. MCTDH-X: *The time-dependent multiconfigurational Hartree for indistinguishable particles software*, http://ultracold.org (2019).
53. Lode, A. U. J. *Tunneling Dynamics in Open Ultracold Bosonic Systems*, Springer Theses, (Springer, Heidelberg, 2014).
54. Lode, A. U. J. Multiconfigurational time-dependent Hartree method for bosons with internal degrees of freedom: Theory and composite fragmentation of multicomponent Bose-Einstein condensates. *Phys. Rev. A* **93**, 063601 (2016).
55. Heimsoth, M. & Bonitz, M. Interacting bosons beyond the Gross–Pitaevskii mean field. *Physica E* **42**, 420 (2010).
56. We divide the dimensional Hamiltonian by $\hbar^2/(mL^2)$ where m is the mass of the considered bosons and L a conveniently chosen length scale.
57. Olshanii, M. Atomic Scattering in the Presence of an External Confinement and a Gas of Impenetrable Bosons. *Phys. Rev. Lett.* **81**, 938 (1998).
58. Sinha, S. & Santos, L. Cold Dipolar Gases in Quasi-One-Dimensional Geometries. *Phys. Rev. Lett.* **99**, 140406 (2007).
59. Cai, Y., Rosenkranz, M., Lei, Z. & Bao, W. Mean-field regime of trapped dipolar Bose-Einstein condensates in one and two dimensions. *Phys. Rev. A* **82**, 043623 (2010).
60. Penrose, O. & Onsager, L. Bose-Einstein Condensation and Liquid Helium. *Phys. Rev* **104**, 576 (1956).
61. Nozieres, P. & James, D. S. Particle vs. pair condensation in attractive Bose liquids. *J. Phys. (France)* **43**, 1133 (1982).
62. Spekkens, R. W. & Sipe, J. E. Spatial fragmentation of a Bose-Einstein condensate in a double-well potential. *Phys. Rev. A* **59**, 3868 (1999).
63. Lode, A. U. J. & Bruder, C. Fragmented Superradiance of a Bose-Einstein Condensate in an Optical Cavity. *Phys. Rev. Lett.* **118**, 013603 (2017).
64. Kramer, P. & Saracen, M. *Geometry of the time-dependent variational principle*, (Springer, Berlin, 1981).
65. Lode, A. U. J., Sakmann, K., Alon, O. E., Cederbaum, L. S. & Streltsov, A. I. Numerically exact quantum dynamics of bosons with time-dependent interactions of harmonic type. *Phys. Rev. A* **86**, 063606 (2012).
66. Gwak, Y., Marchukov, O. V., Fischer, U. R., Benchmarking multiconfigurational Hartree by the exact wavefunction of two harmonically trapped bosons with contact interaction. *arXiv:1811.04705* [cond-mat.quant-gas].
67. Zinner, N. T., Volosniev, A. G., Fedorov, D. V., Jensen, A. S. & Valiente, M. Fractional energy states of strongly interacting bosons in one dimension. *Eur. Phys. Lett.* **107**, 60003 (2014).
68. Kościk, P. & Sowiński, T. Exactly solvable model of two trapped quantum particles interacting via finite-range soft-core interactions. *Scientific Reports* **8**, 48 (2018).
69. Sakmann, K. & Kasevich, M. Single shot simulations of dynamic quantum many-body systems. *Nature Phys* **12**, 451 (2016).
70. Javanainen, J. & Yoo, S. M. Quantum Phase of a Bose-Einstein Condensate with an Arbitrary Number of Atoms. *Phys. Rev. Lett.* **76**, 161 (1996).
71. Castin, Y. & Dalibard, J. Relative phase of two Bose-Einstein condensates. *Phys. Rev. A* **55**, 4330 (1997).
72. Dziarmaga, J., Karkuszewski, Z. P. & Sacha, K. Images of the dark soliton in a depleted condensate. *J. Phys. B* **36**, 1217 (2003).
73. Dagnino, D., Barberán, N. & Lewenstein, M. Vortex nucleation in a mesoscopic Bose superfluid and breaking of the parity symmetry. *Phys. Rev. A* **80**, 053611 (2009).

Acknowledgements

S. Bera acknowledges DST (Govt. of India) for the financial support through INSPIRE fellowship [2015/IF150245] and Rhombik Roy for some useful discussions. B. Chakrabarti acknowledges FAPESP (grant No. 2016/19622-0). AG and MCT acknowledge FAPESP and AG thanks CNPq for financial support. B. Chatterjee acknowledges financial support from the Department of Science and Technology, Government of India under the DST Inspire Faculty fellowship. AUJL and CL acknowledge financial support by the Austrian Science Foundation (FWF) under grant Nos. P 32033 and M 2653, respectively, and the Wiener Wissenschafts- und TechnologieFonds (WWTF) project No. MA16-066.

Author contributions

S.B. conducted the numerical and theoretical investigations, S.B., C.L. and A.U.J.L. wrote the manuscript, A.U.J.L. and C.L. performed complementary calculations, S.B., B. Chak., A.G., M.C.T., M.L.L., B. Chat., C.L., and A.U.J.L. conceived the idea for the project and supported the writeup.

Competing interests
The authors declare no competing interests.

Additional information
Correspondence and requests for materials should be addressed to A.U.J.L.

Reprints and permissions information is available at www.nature.com/reprints.

Publisher's note Springer Nature remains neutral with regard to jurisdictional claims in published maps and institutional affiliations.